Clin Oral Invest (2006) 10: 235–248
DOI 10.1007/s00784-006-0055-2

ORIGINAL PAPER

Frank Du Tré · Reinhilde Jacobs · Sean Styven · Daniel van Steenberghe

Development of a novel digital subtraction technique for detecting subtle changes in jawbone density

Received: 25 November 2005 / Accepted: 3 April 2006 / Published online: 13 June 2006

Abstract The objective of this paper is to develop a novel digital subtraction technique for serial intra-oral radiography, which would allow the detection of subtle variations in grey values. Digital images of the maxilla of a dried human skull and of a fresh pig mandible were acquired using intra-oral photostimulable phosphor plates (Digora FMX, Soredex, Helsinki) with an aluminium calibration step-wedge incorporated in the filmholder. Exposures were made with an X-ray tube for intra-oral radiography (Prostyle Intra, Planmeca, Helsinki). During pilot testing, parameter settings were adapted to reach an optimal contrast. Exposures were repeated within a 1-week interval to determine the test–retest reliability of the development. After in vitro and in vivo testing, the exposure technique and software development were used to evaluate its applicability in a pilot clinical case. Although parameter settings remained stable during the in vitro studies, the clinical exposures yielded non-linear digital images, thus, not readily suitable for data acquisition and comparison of the regions of interest. To allow further analysis, image processing was carried out using self-developed software for semi-automated linearisation and optimised contrast normalisation. This processing significantly increased the precise quantisation of jawbone density and the assessment of subtle bone density changes in arbitrarily selected regions of interest of in vivo exposures. The clinical applicability of the technique is demonstrated in a pilot case. It was demonstrated that minute densitometric deviations could be detected. The present technique and image processing may allow the quantification of jawbone density.

Keywords Radiography · Intra-oral · Subtraction · Calibration · Density

Daniel van Steenberghe is Holder of the P-I Brånemark Chair in Osseointegration.

F. D. Tré · R. Jacobs · S. Styven · D. van Steenberghe (✉)
Department of Periodontology and Oral Imaging Center,
Faculty of Medicine, Katholieke Universiteit Leuven,
Kapucijnenvoer, 7,
3000 Leuven, Belgium
e-mail: Daniel.vanSteenberghe@uz.kuleuven.ac.be

Introduction

Many studies have shown the importance of digital subtraction radiography as a non-invasive means in the detection of subtle bone changes [23, 32]. However, most of the studies are limited to the detection of bone gain or bone loss in phantom simulations [12, 25, 46]. The detection of bone changes under clinical circumstances depends on the geometric and densitometric accuracy [4, 6, 12, 31] of the periodical radiographs. However, local subtle changes in mineral bone content may become unpredictable if the grey-level value range of the digital images does not behave linearly [2]. The use of X-ray densitometry to quantify osseous differences occurring over time is liable to a number of potential difficulties. The most cumbersome among these involves the calibration of essential system elements that are intrinsically non-linear (e.g. X-ray beam, captor response characteristics) and often object-dependent (e.g. scattering effects, soft and hard tissues overlaying the region of interest, ROI) [28]. It has been demonstrated that significant errors can result from inappropriate assumptions underlying the use of calibration schemes based on analyses of radiographs, which directly or indirectly use an external reference with unequal beam attenuation between the reference and the ROI [41]. The use of an aluminium stepwedge and linearisation of a series of images may provide a solution [2]. The present report aims at developing a software for linearisation and contrast enhancement of digital intra-oral radiographs taken in a clinical environment, to enable viewing subtle jawbone density changes.

Materials and methods

The present method for subtraction radiography was developed stepwise, using an extraction socket in a dry

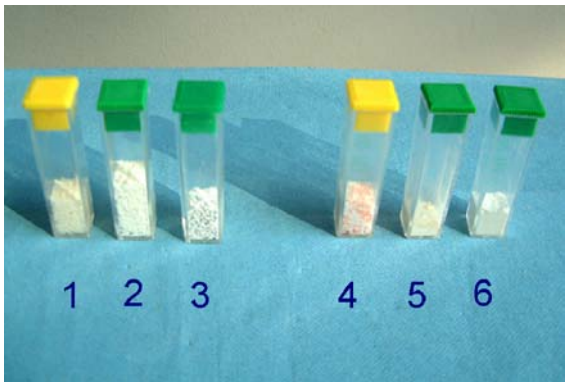

Fig. 1 Standard commercially provided dose of five well-known bone substitute materials and one quantity of ground pig's jawbone as reference (*5*) inserted in square measures of 9×9 mm inside. The *numbers* correspond with the numbers on Fig. 2a,b

human skull and a drilled cavity in a fresh pig's jaw, filled with the materials that will be discussed below. A more detailed description of these approaches has been previously published [11]. This was followed by a trial in a clinical environment.

The following bone substitute materials were used for the present assessment of the novel software (Figs. 1 and 2a,b; Table 1): Biocoral, Inoteb, Saint-Gonnéry, France; BioOss, Geistlich Pharma AG, Wolhusen, Switzerland; Bioplant HTR, Bioplant, South Norwalk, CT, USA; Fisiograft, Ghimas Spa, Bologna, Italy; Frios Algipore, Friadent GmbH, Mannheim, Germany.

Human dried skull with soft tissue simulation

Extraction of the first molar in the right upper jaw of a dried human skull was performed. The socket was then filled and refilled with bone substitute materials of different origin as described. Standardised radiographs were acquired using a beam-aiming device with paralleling technique. All the X-ray exposures were carried out with the same parameter settings. The soft tissues were simulated by means of a rectangular wood setup block (beech) 1-in.-thick (2.54 cm). To ensure the reproducibility of images over time, moulds were made of the upper and lower jaw of the skull. A properly fitting bite block was intra-orally positioned and stabilised by closing the articulation. A cassette holder for the X-ray sensitive phosphor plate and a uniform aluminium reference plate with dimensions 5×6×30 mm for brightness adaptation were incorporated in the bite block. A beam-aiming device with permanent magnets was used to make a stable connection between the bite block and the X-ray tube head. The geometry was controlled by means of small metallic landmarks attached to the cassette at a distance of 10 mm from the captor. Density differences were visualised with a dedicated software for digital subtraction radiography.

Fresh pig's lower jaw including the soft tissues

A cavity was drilled in the molar–premolar region of a pig's lower jaw. The cavity was filled with the same bone substitute materials as described for the dry human skull. Standardised radiographs were acquired using the paralleling technique with adapted beam-aiming device. The soft tissues were preserved and used to simulate the clinical environment. The same aluminium calibration plate as described under human dried skull was used. All the X-ray exposures were taken with the same parameter settings. Density differences were demonstrated with digital subtraction radiography.

Clinical pilot study

The present study reports clinical case material originating from a 1-year follow-up study on bone regeneration. Ethical approval was obtained from the Clinical Trials Committee of the University Hospital (KU Leuven, Leuven, Belgium). Informed consent was obtained. Standardised serial radiographs of the upper jaw of a 57-year-old male patient were acquired at regular intervals according to a standardised protocol. The radiographs were

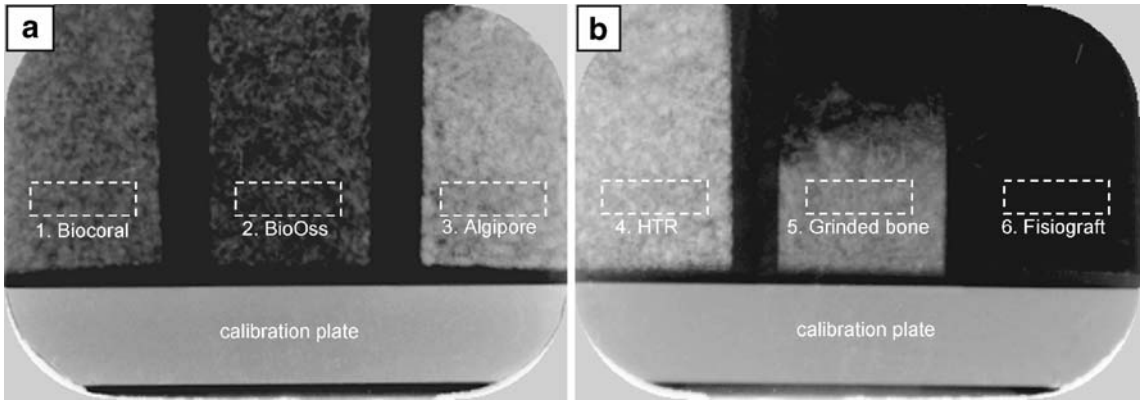

Fig. 2 **a**, **b** Radiographs of the bone substitute materials and the ground pig's jawbone. Measure *6*, although filled, is not visible with classical radiography

Table 1 Characteristics of the bone substitute materials and the ground pig's jawbone as depicted in Figs. 1 and 2a,b

Bone-filling materials	Volume (mm^3)	Weight (mg)	Specific gravity (mg/mm^3)	Density (grey value)
1. Biocoral	10.53	830	78.82	96
2. BioOss	15.39	790	51.33	49
3. Algipore	8.91	440	49.38	151
4. HTR	9.72	680	69.95	146
5. Ground bone	4.86	310	63.78	95
6. Fisiograft sponge	7.29	300	41.15	4

The weight and volume determination occurred on the basis of dry weight without compression. The density in greyscale values is based on the mean greyscale value of the selected rectangular area on the radiographs (Fig. 2a,b). From the data, it can be derived that the specific gravity is not consistent with the density expressed in greyscale values

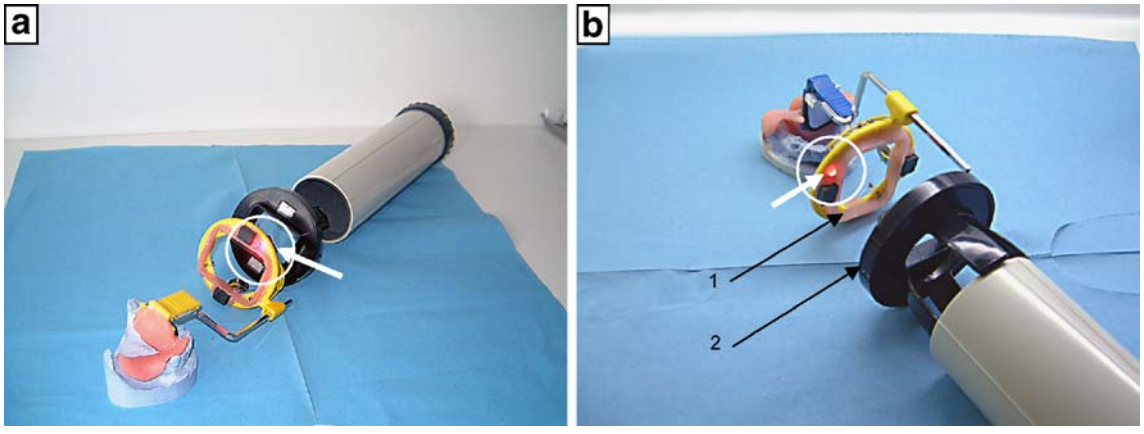

Fig. 3 a, b The figures show the simulation of the electronic detection system with the indicator light bulb (*whitecircle* and *arrow*). As soon as the guiding adapter (*1*) makes contact with the collimator (*2*) over its total surface, the light detector switches on. Conversely, when the contact is interrupted how slightly it may be, the light bulb is extinguished, indicating that the setup of the aiming system has to be retuned before taking radiographs

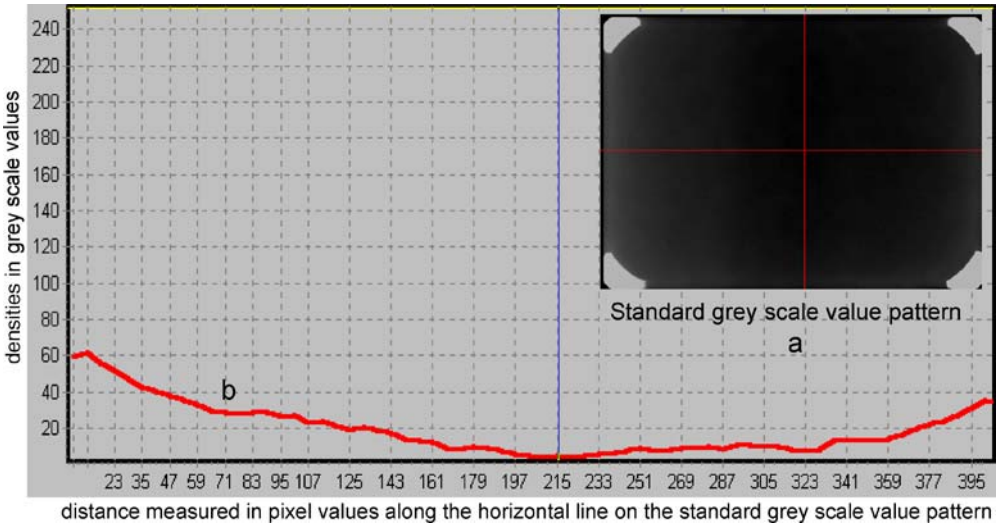

Fig. 4 This figure shows **a** the projection pattern obtained by irradiating, under standardised conditions, a 5-mm thick homogeneous aluminium plate and **b** the shifted density plot measured along the *horizontalline*

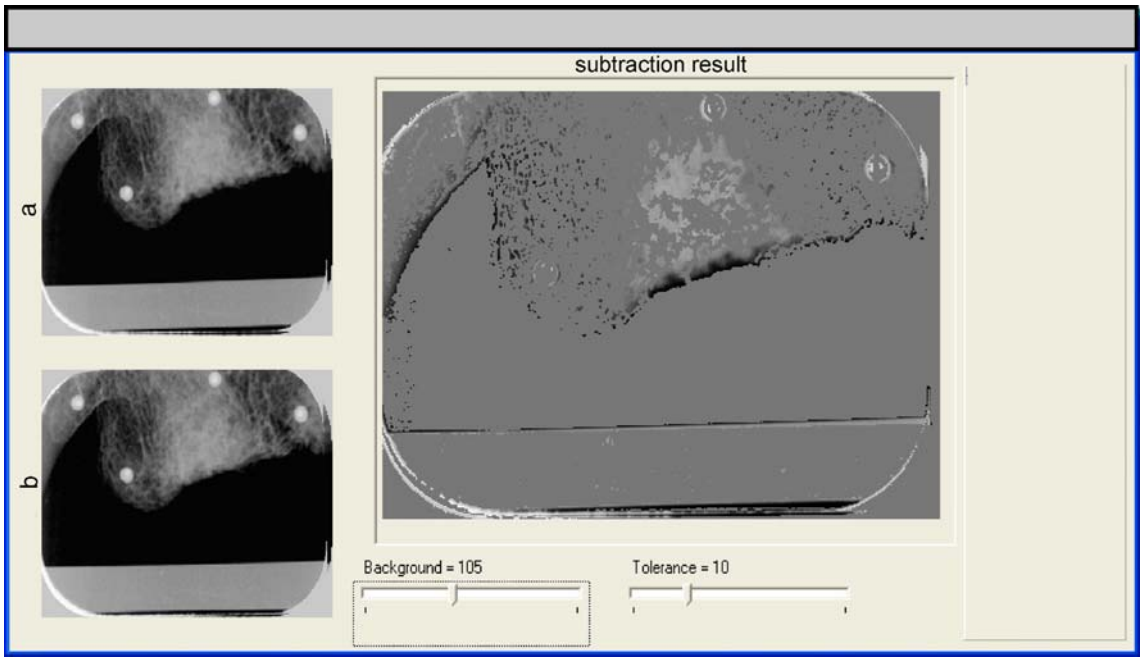

Fig. 5 The subtraction result of an extraction socket of the right upper third molar on a dried human skull filled with high-density bone substitute materials of the same origin is shown: Frios Algipore particle size ∅ 0.3–0.5 mm (**a**) and Frios Algipore particle size ∅ 0.5–1.0 mm (**b**). Density differences between both radiographs can hardly be discerned with classical radiography

obtained after the removal of a remaining root tip in the upper jaw (second premolar) of which the empty socket was filled with bovine bone substitute material (BioOss) and closed with a non-absorbable e-PTFE membrane (Gore-Tex, W.L. Gore and Associates, Flagstaff, AZ, USA) and mucoperiosteal flap. A beam-aiming device with sensor holder (Rinn XCP film holding system, Dentsply Rinn, PA, USA) incorporated in an individualised intra-oral acrylic bite block was aligned according the region of interest to be depicted on the radiographs. Attention was given to aim the central X-ray beam perpendicular to captor and object (paralleling technique) [36]. An aluminium

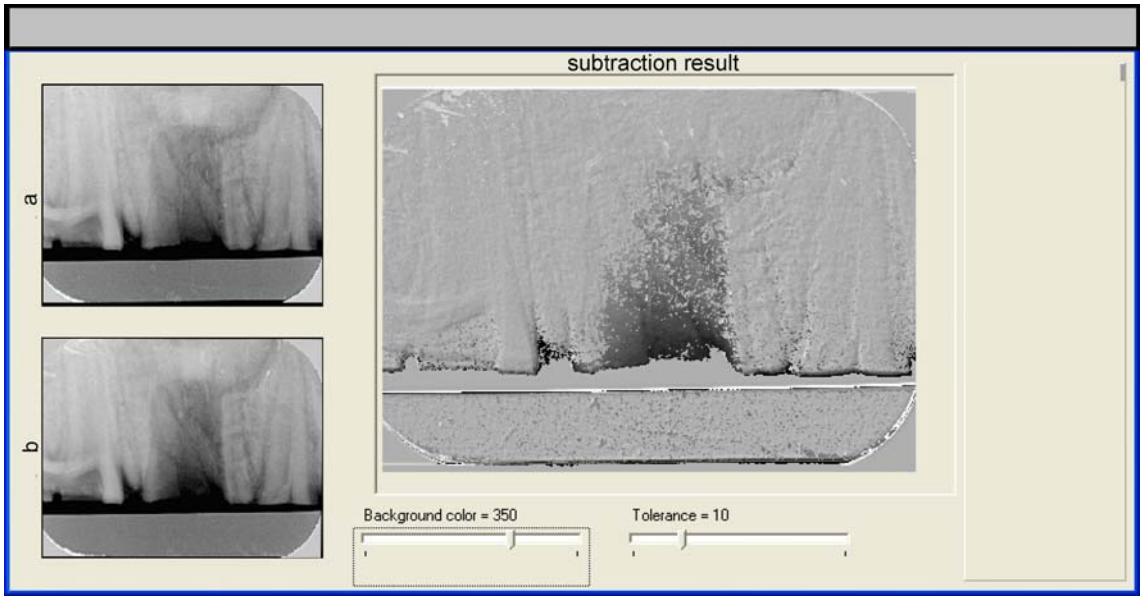

Fig. 6 The cavity drilled at the premolar region of a pig's right lower jaw (for the sake of software, the radiographs are upside down). The cavity has been filled with low-density bone substitute materials of the same origin: Fisiograft powder (**a**) and Fisiograft sponge (**b**). Although no density difference can be discerned between both radiographs with classical radiography, a well-distinguished mottled *outline* appears after subtraction

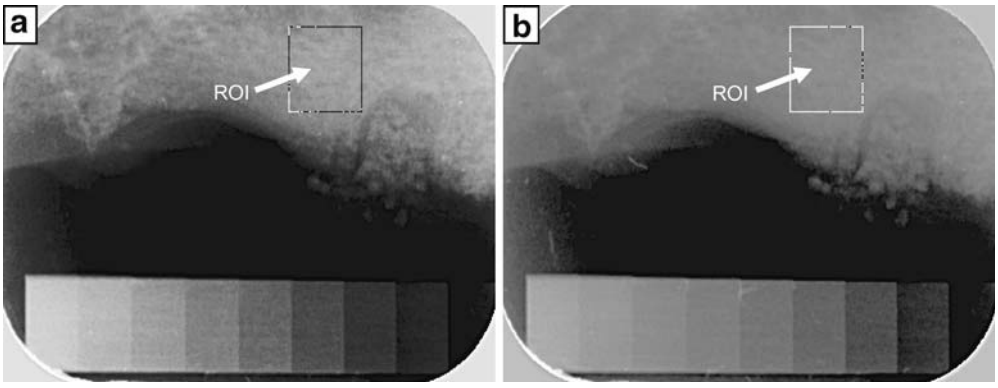

Fig. 7 **a, b** Rectangular area randomly selected (ROI) on both radiographs in the jawbone after simplified grey-level adaptation

Table 2 Mean greyscale values

table 2a (fig. 7a)	
mean greyscale value	
global image	ROI
78.48	144.84
table 2b (fig. 7b)	
mean greyscale value	
global image	ROI
77.34	125.97

calibration stepwedge [28] of nine steps from 1 to 9 mm and a surface area of 3×4 mm^2 per step was built into the captor holder and projected on top of the captor without interference with the jawbone. The rigid connection between the beam-aiming device and tube head, as used in the in vitro experiments, was replaced by a guiding adapter, smoothly positioned against the collimator by two small permanent magnets and controlled by a built-in electronic detection system [18, 19] (Fig. 3a,b).

To limit the damaging interaction of the removable denture worn during the healing period, special attention was paid to the proper adaptation of it. A new standardised radiograph, which had to be taken after 1 week to detect the eventual loss of material because of a dehiscence, allowed the assessment of the reproducibility of the technique. No loss of filling material was found. Densitometric deviations were corrected with the dedicated software using an external reference (aluminium stepwedge). The baseline radiographs are shown to illustrate the accuracy of the processing of clinical images (Figs. 7 and 8a,b).

Photostimulable phosphor plates (21×30 mm blue imaging plates, Digora FMX, Soredex, Helsinki, Finland) were used to the present study. All the radiographs were acquired with a Planmeca Prostyle Intra unit (Planmeca, Helsinki, Finland) with rectangular collimation. The images were produced using a tube voltage of 64 kV, an anode current of 8 mA, a 35-cm focus object distance and an exposure time of 0.2 s.

Processing of the radiographs

Geometric correction The consecutive radiographs, acquired as described above, both in vitro and in vivo, showed a satisfactory geometric stability over time. After superimposition, only a few planar corrections had to be carried out to make the images coincide [13, 19, 33].

Densitometric corrections Whether the radiographs were obtained in vitro or in vivo, in all cases densitometric corrections had to be performed. Distinction was made

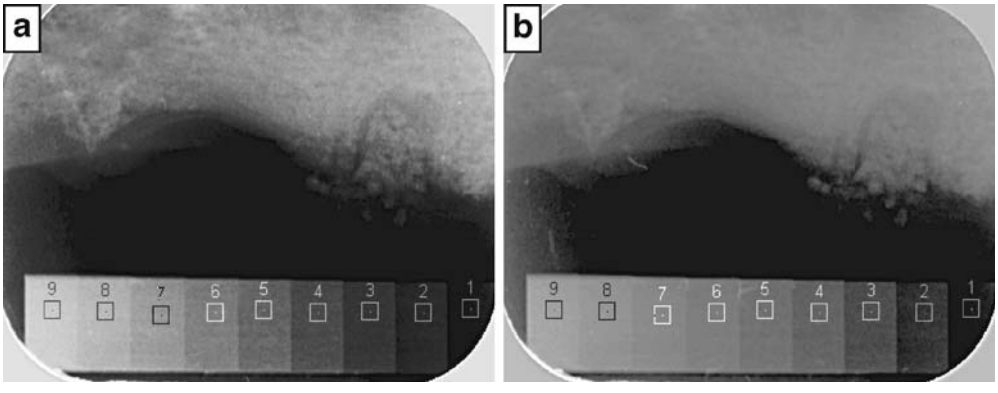

Fig. 8 **a, b** Measuring squares of 14×14 pixels were manually placed in the upper half on each of the nine steps of baseline and follow-up radiograph

Table 3 Measuring values of baseline and follow-up radiographs before image processing

table 3

	a	b	c	d
1	1	1	5	5
2	2	2	18	29
3	3	3	32	60
4	4	4	55	82
5	5	5	81	97
6	6	6	110	109
7	7	7	140	121
8	8	8	176	138
9	9	9	197	152

The range of the baseline radiograph is more stretched, indicating a higher contrast
Column *a* indicates the number of steps
Column *b* indicates the thickness of the aluminium steps in millimeters
Column *c* indicates the density of the steps in greyscale values of the baseline radiograph
Column *d* indicates the density of the steps in greyscale values of the follow-up radiograph

between object-dependent deviations (scattering effects and overlaying of the soft tissues) [8, 24], machine deviations (e.g. non-uniformity of the X-ray beam and scanning unit) [30], variations in parameter settings (e.g. exposure time, kilovoltage, milliamperage) [22, 32] and receptor response characteristics [9]. Scattering patterns (first- and second-order streaks), if present, were only seen for radiographs obtained under clinical circumstances. In most of the cases this kind of localised image contamination could be suppressed by adapting the design of the calibration wedge. Bands caused by X-ray absorption of the soft tissues were mainly limited to the posterior region of the upper jaw, which was beyond the ROI's considered. Machine deviations [14] caused a recurrent pattern in grey-value distribution for a specific projection geometry (Fig. 4). This pattern was recorded by irradiating a 5-mm thick homogeneous aluminium plate under standardised conditions as described before. The procedure was repeated 50 times, and the mean value of the distribution pattern was computer-calculated and adapted to each radiograph according to three measuring points on the stepwedge and then subtracted. In this way, the linear characteristics of the radiographs were roughly restored.

Fluctuations in parameter settings and differences in sensor response characteristics, mainly occurring when dealing with clinical radiographs taken over time, are additional non-linear factors that can lead to inaccuracies in estimates of bone mass [28]. In pilot experiments, it appeared that parameter settings and sensor characteristics were much better controllable for radiographs acquired in laboratory conditions than in clinical conditions [6, 32]. Grey-level normalisation for the first group (laboratory conditions) was performed through simple brightness adaptation by adding or subtracting the difference between the calibration plates to or from the follow-up radiographs. The same did not hold for the second setting (clinical conditions). The radiographs were much more parameter-sensitive, and the grey-level normalisation was comparatively more complex [1]. The sequential steps followed in grey-level normalisation for the clinical group were linearisation, brightness and contrast adaptation, and contrast optimisation. These computer-based techniques appeared to be essential when minute density changes between baseline and follow-up radiographs had to be evaluated.

Results

The simplified method of brightness adaptation appeared to be reliable for radiographs acquired under in vitro conditions as demonstrated on Figs. 5 and 6.

From the study on the dry human skull and the fresh pig's jaw, it appeared that the standardisation of image acquisition and the novel software were very promising. The test results were encouraging to further refine the digital calibration and subtraction techniques in a clinical environment through a pilot case.

However, it must be understood that these results cannot immediately be transferred to the clinical situation [1, 2]. The procedure turned out to be inaccurate for radiographs obtained under clinical circumstances, and more advanced computer techniques have to be developed to make them appropriate for the detection of minute bone density changes. To evaluate the stability of parameter settings under clinical circumstances, both a simplified method of brightness adaptation and an advanced procedure of grey-level normalisation were performed.

The principle of simplified normalisation is illustrated in a clinical case report (Fig. 7a,b). After superimposing the radiographs, an area was manually selected on the calibration plates, and the mean density of it in greyscale values was computer-calculated. The overall brightness of the radiographs was corrected according to the simplified procedure. To evaluate the accuracy of it, a ROI was arbitrarily selected on the radiographs in the jawbone. The mean density value for each ROI was supposed to be the same because the time interval of acquisition (1 week) was too short for bone remodelling. The data on Table 2a,b prove the inaccuracy of the method for radiographs acquired under clinical circumstances.

To underline the accuracy of advanced densitometric normalisation of clinical serial radiographs, the same radiographs were used. The mean greyscale value of each step of the stepwedge was measured by manually placing a measuring square of 14×14 pixels in the upper half of the steps (Fig. 8). The data collected (Table 3) were used to plot a graph in a two-dimensional coordinate system (Fig. 9a,b). The thickness of each aluminium step was plotted against

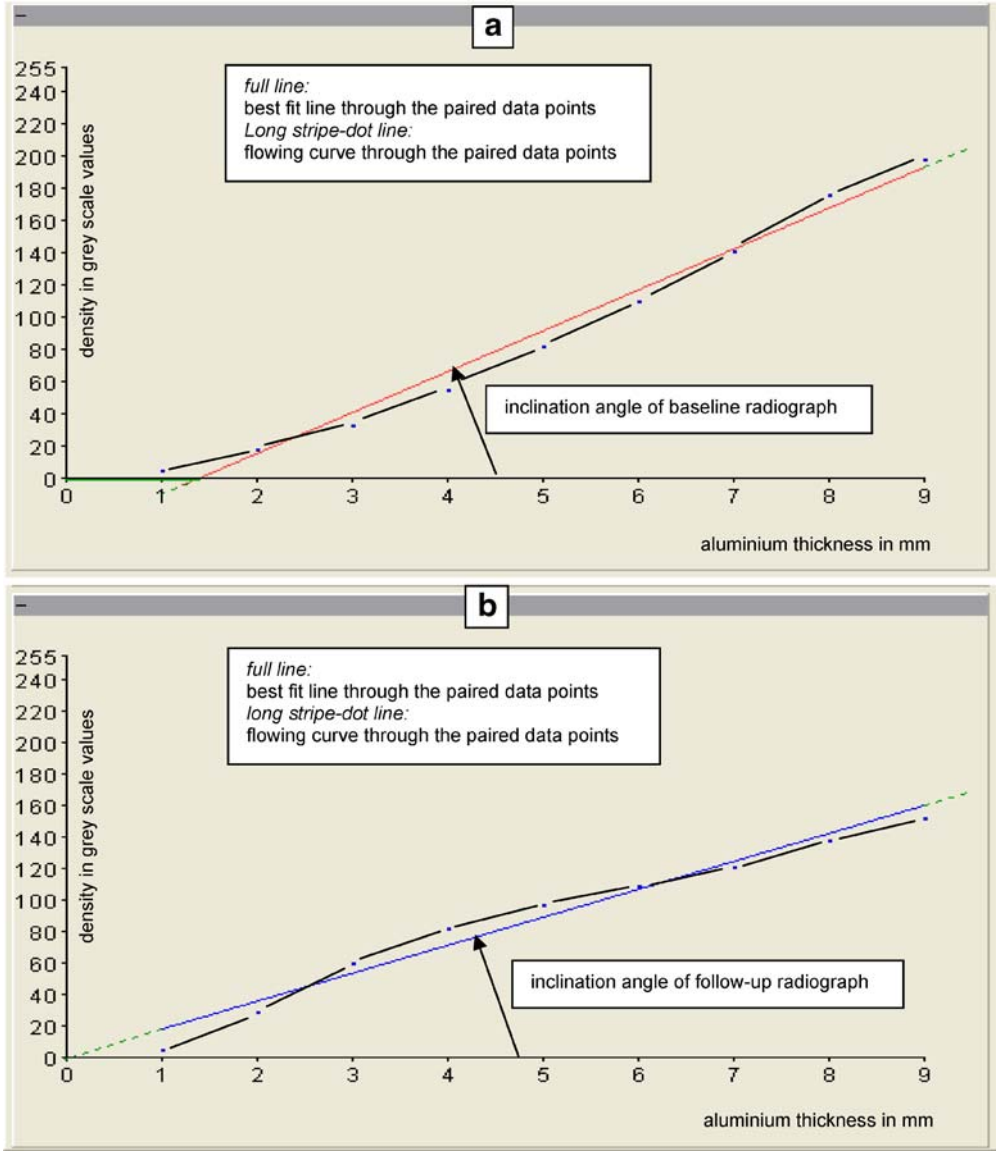

Fig. 9 **a**, **b** The paired data from Table 3 are displayed as *darkdots*. A *flowingcurve* is plotted by smoothly connecting the paired data points. The best fit line is drawn through the paired data points and extended to the extremes of the graph paper. The inclination angle of the best-fit line of the baseline radiograph is steeper as the corresponding angle of the follow-up radiograph, indicating that the image contrast of the baseline radiograph is higher than that of the follow-up radiograph

its mean greyscale value. The coordinate points were connected by a flowing curve, and the best-fit line was calculated by regression and drawn through the points. The slopes of the regression lines appeared to deviate from each other. The steepness of the slope is a measure for the contrast, affecting the mean density of the region of interest. The flowing curve through the coordinate points was equalised with the linear best-fit line. This way, the digital image was linearised and the predictability of the bone density of a local region in the global image was increased. A theoretical stepwedge was computer-simulated (Table 4a,b; Fig. 10). The greyscale range was maximally stretched (contrast enhancement). The paired data were chosen such that the sequence was linear over the total range. This theoretical model was used as the standard to which all the serial radiographs were conformed. This way, the contrast and brightness of the radiographs were matched with optimal contrast enhancement (Table 5). To evaluate the accuracy of this procedure, a randomly chosen rectangular ROI was selected on both radiographs (Fig. 11a,b) and the mean density value was computer-calculated (Table 6a,b; Fig. 12). The results could even be improved by taking advantage of computer automation. The most representative part of each aluminium step was computer-determined (instead of manually assessed). On this basis, the steps of the aluminium stepwedge were computer-reconstructed (Fig. 13a,b). Each step was now homogeneous, and the positioning of the measuring squares was no longer critical. Given the precision required in mass estimation, the processing of the images was repeated by the same operator to confirm that the results were consistent and reproducible [28].

Table 4 **a, b** Coordinate points of the theoretical linear stepwedge

Table 4a

Step	Grey scale value (total range 0 -255)
1.	5
2.	32
3.	59
4.	86
5.	113
6.	140
7.	167
8.	194
9.	221

Table 4b

Step	Thickness (mm)
1.	1
2.	2
3.	3
4.	4
5.	5
6.	6
7.	7
8.	8
9.	9

The thickness of the theoretical steps is kept equal to the thickness of the real aluminium stepwedge. To optimise contrast and brightness, the greyscale values of the theoretical steps were stretched towards the upper limit. The graphical curve, being a straight line through all of the paired data points, is used as the standard for all the serial radiographs

Table 5 Measuring values of baseline and follow-up radiographs after adaptation to the theoretical stepwedge (cf. Table 4a)

table 5

a	b	c	d
1	1	4	8
2	2	32	31
3	3	60	58
4	4	86	85
5	5	113	113
6	6	139	141
7	7	167	167
8	8	194	194
9	9	222	221

Column *a* indicates the number of steps
Column *b* indicates the thickness of the aluminium steps in millimeters
Column *c* indicates the density of the steps in greyscale values of the baseline radiograph
Column *d* indicates the density of the steps in greyscale values of the follow-up radiograph

Simplified grey-level adaptation

The measuring results appeared to be reproducible. Only minute insignificant differences remained. Although the mean greyscale value of the global image of the follow-up radiograph was very close to that of the baseline radiograph after brightness adaptation, the computer-calculated mean greyscale value for the ROI's were strongly varying (Table 2a,b). This demonstrates the inaccuracy of simplified digital image processing when dealing with differences in contrast, as can be derived from the difference in steepness of the regression lines (Fig. 9a,b).

Advanced grey-level normalisation with linearisation and contrast optimisation

The measuring results again appeared to be reproducible. The study tested the assumption that estimates of bone mass must be identical for serial radiographs taken within a short time interval (1 week) because no bone changes take place within this period of time. From Fig. 9a,b, it can be observed that, besides variations in contrast and brightness (slope angle and vertical shift of the least squares lines of fit), the linearity of the serial radiographs was disturbed (non-linear curve through the coordinate points). Table 3 shows the greyscale values and the greyscale range of the aluminium steps before image processing (5 to 197 and 5 to 152). The range of the follow-up radiograph is more compressed with respect to the baseline radiograph, which points to a lower contrast. Table 5 shows the greyscale values and the greyscale range of the aluminium steps after conforming the radiographs to the theoretical stepwedge (4 to 222 and 8 to 221 compared to 5 to 197 and 5 to 152, respectively). At this stage of image processing, the greyscale values of the aluminium steps were very close to each other and to the theoretical stepwedge (cf. Table 4a). Figure 12a,b show the plots of the paired data after image processing. From the graphs it can be observed that (1) the coordinates of the plots are situated on a straight line, (2) the plots have the same slope steepness, (3) the

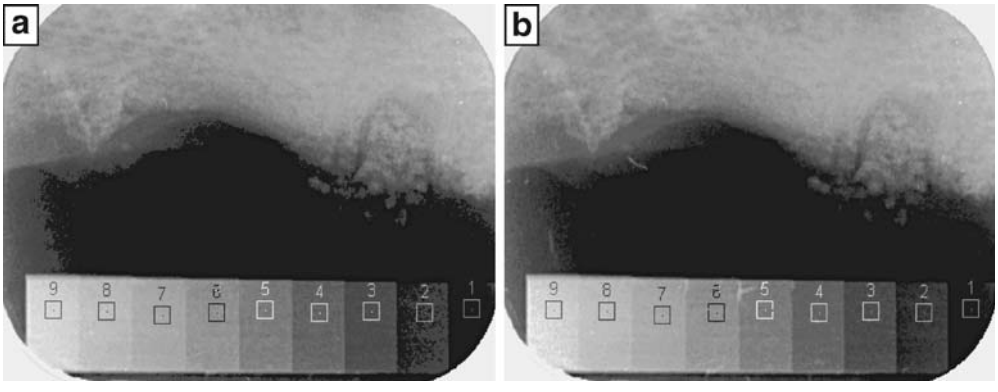

Fig. 10 **a, b** The radiographs after adaptation to the theoretical stepwedge are shown

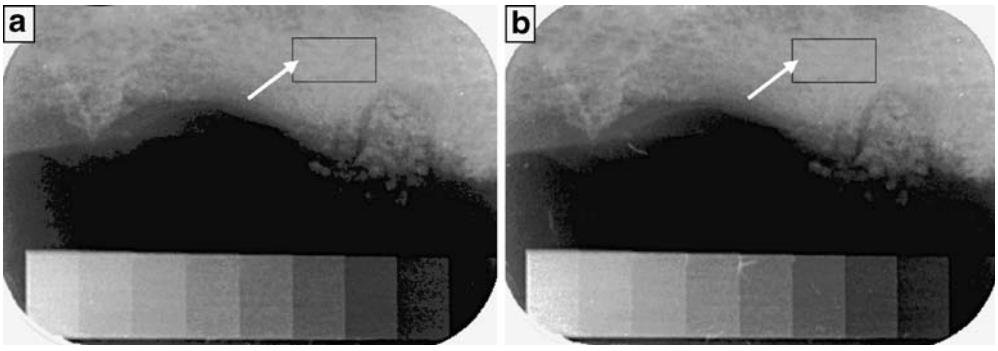

Fig. 11 **a, b** Arbitrarily chosen ROI on the jawbone indicated by the *whitearrow*

plots are on the same level, and (4) the steepness of the slope is enhanced (cf. with Fig. 9a,b). These characteristics of the radiographs after processing prove that (1) the linearity of the radiographs has been restored, (2) the contrast of the radiographs has been normalised, (3) the brightness of the radiographs has been normalised, (4) the contrast of the radiographs has been optimised. The accuracy of the image processing was evaluated by comparing the mineral bone content of the arbitrarily selected ROI's (Fig. 14a,b). Table 6a,b shows that the densities expressed in greyscale values for both radiographs are 178 and 179, respectively, and the corresponding aluminium equivalent thicknesses are 7.44 and 7.41 mm. Table 7 indicates the results after computer-aided reconstruction of the aluminium steps. Both the greyscale range and the intermediate greyscale values of the steps are equal to each other and to the theoretical stepwedge (cf. Table 4a). Figure 15a,b illustrates that the best-fit lines through the paired data points are straight lines coinciding with each other. Tables 8a,b show that the mean densities of the ROI's in greyscale values and in aluminium equivalent values are 172 to 172 and 7.19 to 7.19 mm, respectively, proving the accuracy of the advanced digital image processing.

Discussion

The present research enabled in vitro and in vivo validation of a technique for digital subtraction radiography. The primary goal of the dedicated software tool was to monitor subtle jawbone density changes. It was assumed that deviations in the normalisation of the grey-level values had to be restricted within very narrow limits [15]. The detection of minute densitometric bone changes under clinical circumstances also depends on the accuracy of the projection geometry [6, 37]. To overcome any variation in projection geometry, standardised radiographs were acquired using an electronic-controlled beam-aiming device with paralleling technique and individualised bite blocks [10, 19, 48]. Stable acquisition of serial radiographs and monitoring of subtle changes in bone mineral content is not evident when dealing with film positioning in edentulous jawbone [17]. Therefore, as suggested by some investigators, the individual bite blocks were expanded allowing the utilisation of a larger mucosal support in a more stable area of the jaws [10, 13] and further away from the ROI. Robust image registration is of great importance as it is impossible to manipulate images in the computer of a two-dimensional representation from a different angle of a three-dimensional object, without additional information on the three-dimensional relationship between structures [12].

Normalisation of the grey-level values was performed through linearisation, contrast-brightness adaptation and contrast optimisation on the basis of an external reference (aluminium stepwedge). The advantage of an external reference is absolute normalisation, allowing the straightforward determination of quantitative measurements such as changes in bone volume [26]. Furthermore, the two-wedge method, i.e. using a reference wedge in each of the radiographs of the subtraction pair, was used. According to Ruttiman and Webber [35], the single-wedge method is superior if there is linearity between the reference height and the grey level. However, an analysis by Allen and Hausmann [2] comparing both methods concluded that the criterion of linearity is mainly met in in vitro studies; consequently, the two-wedge method is preferable for in vivo studies. Automatic greyscale adjustment, as proposed by different researchers, does not seem useful for the detection of small bone lesions [40].

An important issue is the predictability of the greyscale distribution, which is directly related to the linearity of the digital images [29]. Greyscale linearisation is the adjustment of brightness relationships among the objects in an image. The purpose of greyscale linearisation is to render faithfully the different brightness values in an image. It is

Table 6 **a, b** Mean density in greyscale values and in aluminium equivalent values of the ROI's

a	
Mean density of the ROI in greyscale values	
Figure 12a	179
Figure 12b	178
b	
Mean density of the ROI in aluminium equivalent values	
Figure 12a	7.44 mm
Figure 12b	7.41 mm

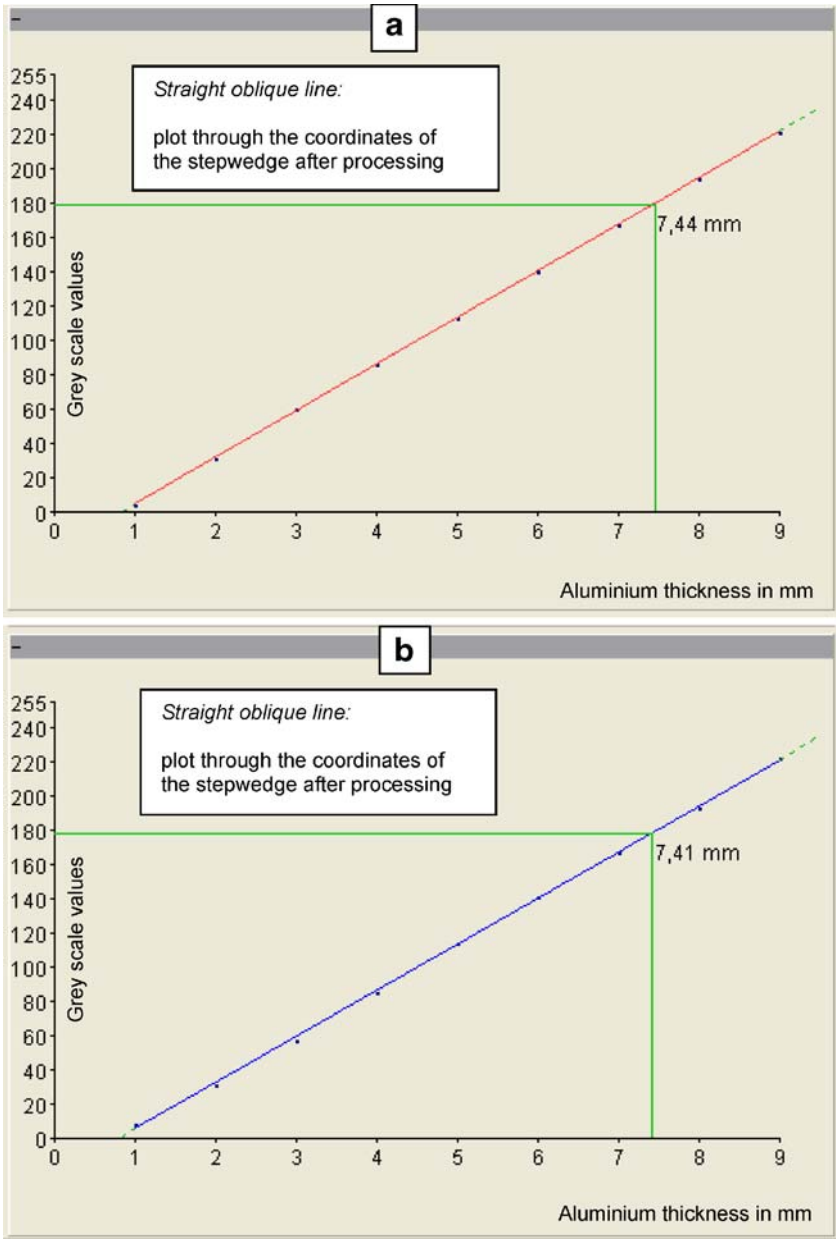

Fig. 12 **a, b** Graphical presentation of the mean density value of the ROI's

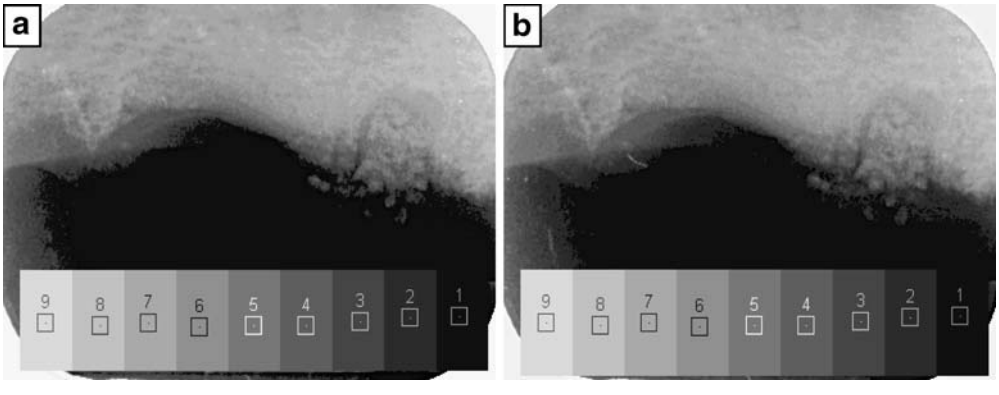

Fig. 13 **a, b** Computer reconstruction of the stepwedges

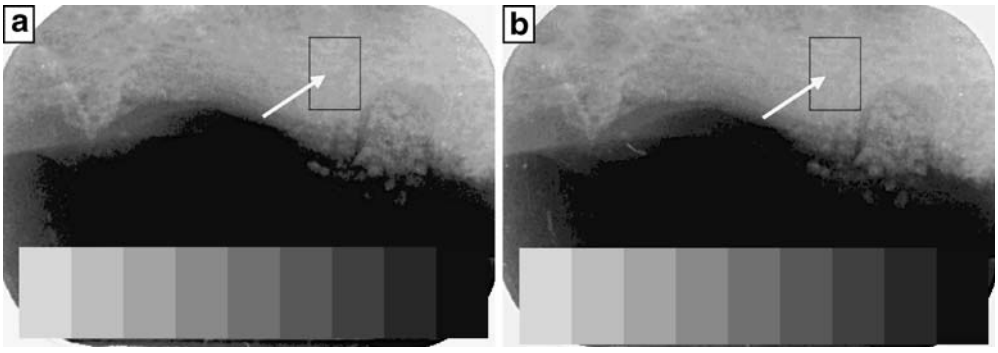

Fig. 14 **a, b** Arbitrarily chosen ROI on the jawbone indicated by the *whitearrow*

commonly assumed that the other objects in the image will be put in their proper brightness relationships as well. Improper greyscale linearisation can render brightness values inaccurately so that objects may appear brighter or darker than they actually appeared when the image was recorded. Without linearisation it may be possible that differences in greyscale values are measured between the ROI's even for radiographs acquired within a short time interval and after normalisation of the grey tones. The classical assumptions (being stationary, linearity, etc.) do not apply to clinical situations [7]. Radiographic image quality is subject to variations in beam intensity including X-ray scattering and anode heel effect [5]. It appeared that the design of the aluminium stepwedge played a key role in the suppression of the scattering effects [3]. To overcome the inhomogeneity of the X-ray beam [30, 38] and the receptor system [9], a standard pattern based on the overall greyscale distribution was generated and subtracted from the global images. Finally, all clinical radiographs acquired over time are susceptible to fluctuations in parameter settings [21]. Likar and Pernus [27] tested the efficacy of the three most often used contrast correction methods to reduce contrast mismatches that can adversely affect digital subtraction in dental radiography. Experiments showed that (1) 'optical density thickness function' (ODTF) method, which is based on a function relating grey-level values of the aluminium wedge image and the corresponding thicknesses of the wedge, induced less contrast correction error than most accepted methods. Those are (2) the 'cumulative density function' method based on matching the cumulative histogram of the follow-up radiographs to the baseline radiograph and (3) the 'least square quadratic approximation' method [34]. The latter is based on plotting the grey levels of all pairs of pixels having the same spatial coordinates in both images in the two-dimensional space to use the quadratic polynomial regression curve through the coordinate points as mapping function between grey-level values of the two images. Opposite to the other methods, the ODTF method is able to detect more subtle bone changes and allows better bone change volume estimations. In the present study, a variant of the ODTF method was developed. Instead of directly matching the ODTF's of baseline with that of follow-up radiographs, they were matched to a theoretical optimised ODTF. This is done after having been equalised with their individual linear regression curve of best fit. Although a conventional skeletal dual X-ray energy absorptiometry scanner and a dual-photon absorptiometry scanner developed by Wowern [42–44] were successfully used for the measurements of bone mineral density and bone mineral content in the human jaws [45], the present method allows to detect even localised subtle changes. The normalisation method, as proposed in the present study, tended to be accurate and reliable.

By conforming the serial radiographs to a theoretical model, grey-level normalisation and contrast optimisation of the serial radiographs could be performed. Contrast enhancement is important for the perception of small contrast details, especially in the low-exposure range [47]. However, when the contrast enhancement exceeds certain limits, irreversible loss of originality of the quantitative data occurs [16]. Contrast optimisation is a function of the steepness of the regression line through the coordinate points of the aluminium stepwedge [20] (Fig. 9a,b). Therefore, the slope angle of the theoretical model may not exceed certain limits. These limits can be derived from the greyscale distribution as displayed on the histogram. Experimentally, it appeared that the increase of the slope angle or the stretching of the

Table 7 Measuring values of baseline and follow-up radiographs after computer-aided stepwedge reconstruction (cf. Table 4a)

Table 7

a	b	c	d
1	1	5	5
2	2	32	32
3	3	59	59
4	4	86	86
5	5	113	113
6	6	140	140
7	7	167	167
8	8	194	194
9	9	221	221

Column *a* indicates the number of steps
Column *b* indicates the thickness of the aluminium steps in millimeters
Column *c* indicates the density of the steps in greyscale values of the baseline radiograph
Column *d* indicates the density of the steps in greyscale values of the follow-up radiograph

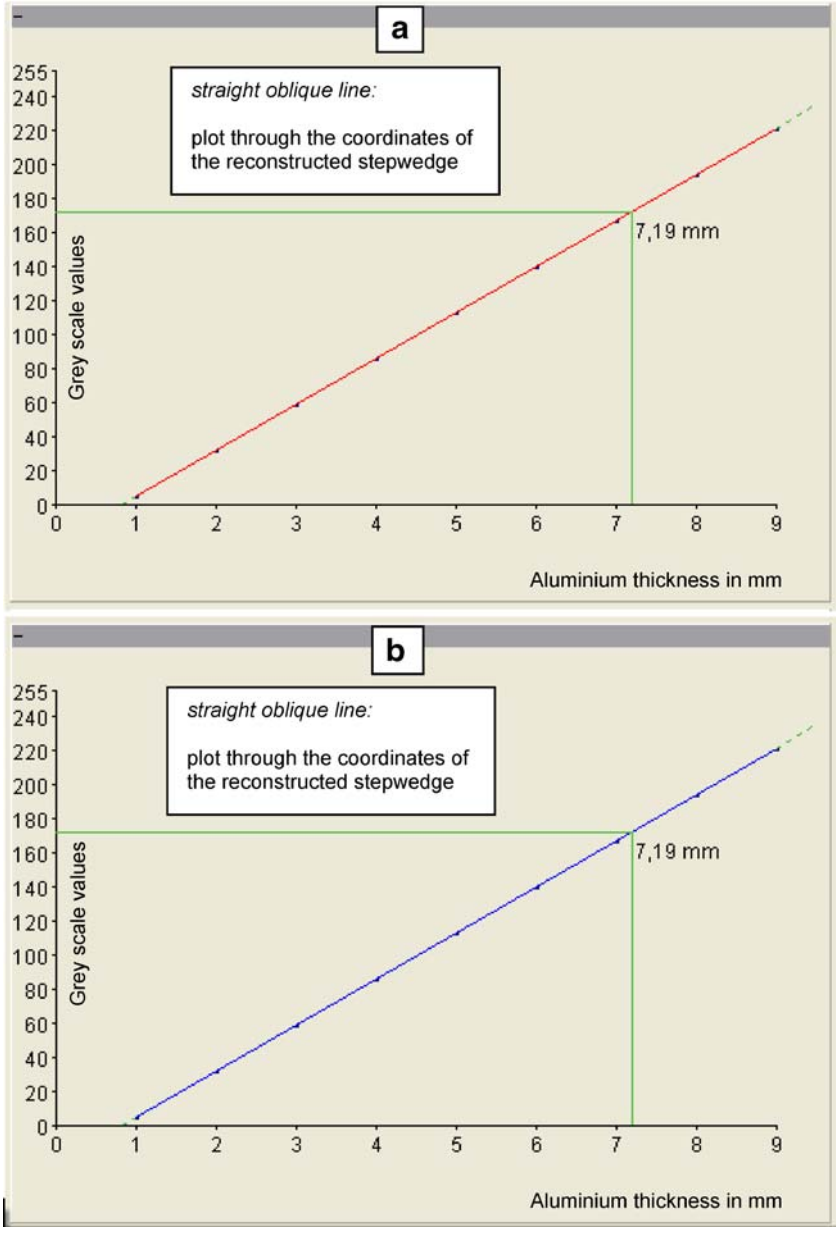

Fig. 15 a, b Graphical presentation of the mean density of the ROI's expressed in greyscale values and in aluminium equivalent values after stepwedge reconstruction

greyscale range towards the upper limit of the grey tones is less sensitive for image loss than towards the lower limit. An important improvement in grey-level correction was the computerised search of the most representative part of each aluminium step, which was a clear improvement towards the manual determination [39].

Conclusions

The presently developed technique and dedicated software tool should allow to lower the threshold of bone density variations on subtracted radiographs. Preliminary data validate the appropriateness of the technique for collecting reproducible in vivo images of the jawbone.

Table 8 a, b Mean density in greyscale values and in aluminium equivalent values of the ROI's, proving the accuracy of the methodology

a	
Mean greyscale value of the ROI	
Figure 15a	172
Figure 15b	172
b	
Aluminum equivalent value of the ROI	
Figure 15a	7.185 mm
Figure 15b	7.185 mm

References

1. Allen K, Emrich L, Piedmonte M, Hausmann E (1992) Relationship of texture measurements to the prediction of correct evaluation in subtraction radiography. J Periodontal Res 27:197–206
2. Allen KM, Hausmann E (1996) Analytical methodology in quantitative digital subtraction radiography: analyses of the aluminum reference wedge. J Periodontol 67:1317–1321
3. Amendolia SR, Bisogni MG, Delogu P, Fantacci ME, Marchi A, Novelli M, Oliva P, Quattrocchi M, Rosso V, Stefanini A, Zucca S (2002) Experimental study of Compton scattering reduction in digital mammographic imaging. IEEE Trans Nucl Sci 49:2361–2365
4. Benn DK (1990) Limitations of the digital image subtraction technique in assessing alveolar bone crest changes due to misalignment errors during image capture. Dentomaxillofac Radiol 19:97–104
5. Carlton RR, Adler AM (1996) Principles of radiographic imaging, 2nd edn. Delmar, Albany, NY, p 730
6. Christgau M, Hiller KA, Schmalz G, Kolbeck C, Wensel A (1998) Quantitative digital subtraction radiography for the determination of small changes in bone thickness: an in vitro study. Oral Surg Oral Med Oral Pathol Oral Radiol Endod 85:462–472
7. Coatrieux JL (2002) Signal processing and physiological modeling—part 1: surface analysis. Crit Rev Biomed Eng 30:9–35
8. Couture RA, Hildebolt C (2000) Quantitative dental radiography with a new photostimulable phosphor system. Oral Surg Oral Med Oral Pathol Oral Radiol Endod 89:498–508
9. Couture RA, Hildebolt CFR (2002) Precise image-receptor calibration and monitoring of beam quality with a step wedge. Dentomaxillofac Radiol 31:56–62
10. Couture RA, Dixon DA, Hildebolt CF (2005) A precise receptor-positioning device for subtraction radiography, based on cross-arch stabilisation. Dentomaxillofac Radiol 34:231–236
11. Du Tré F (2004) Applicability of radiologic analytical methods to evaluate the healing efficiency of extraction sockets using bone substitute materials. Master Thesis, Catholic University Leuven, Department of Periodontology, Leuven, Belgium, pp 146
12. Ellwood RP, Davies RM, Worthington HV (1997) Evaluation of a dental subtraction radiography system. J Periodontal Res 32:241–248
13. Engelke W, de Valk S, Ruttimann U (1990) The diagnostic value of subtraction radiography in the assessment of granular hydroxylapatite implants. Oral Surg Oral Med Oral Pathol Oral Radiol Endod 69:636–641
14. Jean A, Epelboin Y, Rimsky A, Soyer A, Ouhayoun JP (1996) Digital image ratio: a new radiographic method for quantifying changes in alveolar bone. Part 1: theory and methodology. J Periodontal Res 31:161–167
15. Griffiths GS, Brägger U, Fourmousis I, Sterne JAC (1996) Use of an internal standard in subtraction radiography to assess initial periodontal bone changes. Dentomaxillofac Radiol 25:76–81
16. Guneri P, Lomcali G, Boyacioglu H, Kendir S (2005) The effects of incremental brightness and contrast adjustments on radiographic data: a quantitative study. Dentomaxillofac Radiol 34:20–27
17. Handschel J, Kleinheinz J, Kelker M, Reuter I, Joos U (1999) Reproducible X-ray projection geometry in edentulous patients. Dentomaxillofac Radiol 28:368–371
18. Hausmann E, Kutlubay ME, Odrobina D et al (1995) Studies on the angular reproducibility of positioning patients adjacent to an X-ray tube 2. A new electronically guided force-sensitive sensor-based alignment system. J Periodontal Res 30:294–297
19. Hausmann E, Allen K, Loza J, Buchanan W, Cavanaugh PF Jr (1996) Validation of quantitative digital subtraction radiography using the electronically guided alignment device/impression technique. J Periodontol 67:895–899
20. Hayakawa Y, Farman AG, Scarfe WC, Kuroyanagi K, Rumack PM, Schick DB (1996) Optimum exposure ranges for computed dental radiography. Dentomaxillofac Radiol 25:71–75
21. Helmrot E, Carlsson GA, Eckerdal O (1994) Effects of contrast equalization on energy imparted to the patient: a comparison of two dental generators and two types of intraoral film. Dentomaxillofac Radiol 23:83–90
22. Hildebolt CF, Fletcher G, Yokoyama-Crothers N, Conover GL, Vannier MW (1997) A comparison of the response of storage phosphor and film radiography to small variations in X-ray exposure. Dentomaxillofac Radiol 26:147–151
23. Janssen PTM, van Palenstein Helderman WH, van Aken J (1989) The detection of in vitro produced periodontal bone lesions by conventional radiography and photographic subtraction radiography using observes and quantitative digital subtraction radiography. J Clin Periodontol 16:335–341
24. Kitagawa H, Farman AG, Sheetz JP , Brown WP, Lewis L, Benefiel M, Kuroyanagi K (2000) Comparison of three intraoral storage phosphor systems using subjective image quality. Dentomaxillofac Radiol 29:272–276
25. Lee SS, Huh YJ, Kim KY, Heo MS, Choi SC, Koak JY, Heo SJ, Han CH, Yi WJ (2004) Development and evaluation of digital subtraction radiography computer program. Oral Surg Oral Med Oral Pathol Oral Radiol Endod 98:471–475
26. Lehmann TM, Grondahl HG, Benn DK (2000) Computer-based registration for digital subtraction in dental radiology. Dentomaxillofac Radiol 29:323–346
27. Likar B, Pernus F (1997) Evaluation of three contrast correction methods for digital subtraction in dental radiography: an in vitro study. Med Phys 24:299–307
28. Loftin R, Webber R, Horton R, Tyndall D, Moriarty J (1998) Effect of projective aspects variations on estimates of changes in bone mass using digital subtraction radiography. J Periodontal Res 33:352–358
29. Marino A (2000) Chaos and fractals in biology and medicine. Temple presentation. Temple University, Center for Frontier Science, 22 March 2000
30. Markov VT, Fetisov GV, Zhukov SG (1990) Corrections for absorption and beam inhomogeneity in X-ray single-crystal diffractiometry: method of analytical integration. J Appl Crystallogr 23:94–98
31. Mol A, Dunn SM (2003) Effect of bone chip orientation on quantitative estimates of changes in bone mass using digital subtraction radiography. J Periodontal Res 38:296–302
32. Mol A, Dunn SM (2003) The performance of projective standardization for digital subtraction radiography. Oral Surg Oral Med Oral Pathol Oral Radiol Endod 96:373–382
33. Nummikoski PV, Martinez TS, Matteson SR, McDavid WD, Dove SB (1992) Digital subtraction radiography in artificial recurrent caries detection. Dentomaxillofac Radiol 21:59–64
34. Ohki M, Okano T, Yamada N (1988) A contrast-correction method for digital subtraction radiography. J Periodontal Res 23:277–280
35. Ruttiman UE, Webber RL (1987) Volumetry of localized bone lesions by subtraction radiography. J Periodontal Res 22:215–216
36. Schulze RK, d'Hoedt B (2001) Mathematical analysis of projection errors in "paralleling technique" with respect to implant geometry. Clin Oral Implants Res 12:364–371
37. Sewerin I (1990) Device for serial intraoral radiography with controlled projection angles. Tandlaegebladet 15:613–617
38. Syriopoulos K, Velders XL, Geraets WG, van der Stelt PF (1998) A radiographic method for measuring radiation dose based on beam quality. Dentomaxillofac Radiol 27:287–292
39. Tagger M, Katz A (2003) Radiopacity of endodontic sealers: development of a new method for direct measurement. J Endod 29:751–755
40. Versteeg CH, Sanderink GC, van Ginkel FC, van der Stelt PF (1998) Effects of calibration and automatic greyscale adjustment on detectability of simulated bone lesions using a storage phosphor system. Dentomaxillofac Radiol 27:240–244
41. Webber RL, Ruttimann UE, Heaven TJ (1990) Calibration errors in digital subtraction radiography. J Periodontal Res 25:268–275

42. von Wowern N (1985) Dual-photon absorptiometry of mandibles: in vitro test of a new method. Scand J Dent Res 93:169–177
43. von Wowern N (1985) In vivo measurement of bone mineral content of mandibles by dual-photon absorptiometry. Scand J Dent Res 93:162–168
44. von Wowern N, Worsaae N (1988) Bone mineral content of the maxilla estimated by dual-photon absorptiometry after augmentation with bone or hydroxyapatite. J Dent Res 67:1405–1408
45. von Wowern N (2001) General and oral aspects of osteoporosis:a review. Clin Oral Investig 5:71–82
46. Yoshioka T, Kobayashi C, Suda H, Sasaki T (1997) Quantitative subtraction with direct digital dental radiography. Dentomaxillofac Radiol 26:286–294
47. Yoshiura K, Welander U, Shi XQ, Li G, Kawazu T, Tatsumi M, Okamura K, McDavid WD, Kanda S (2001) Conventional and predicted perceptibility curves for contrast-enhanced direct digital intraoral radiographs. Dentomaxillofac Radiol 30:219–225
48. Zappa U, Simona C, Graf H, van Aken J (1991) In vivo determination of radiographic projection errors produced by a novel film holder and an X-ray beam manipulator. J Periodontol 62:674–683